CHARACTERIZING PHYSICAL PROPERTIES AND OCEAN CURRENTS IN THE EASTERN ROSS SEA, ANTARCTICA

A Senior Scholars Thesis

by

GENEVIEVE VICTORIA GENEST

Submitted to Honors and Undergraduate Research
Texas A&M University
in partial fulfillment of the requirements for the designation as

UNDERGRADUATE RESEARCH SCHOLAR

May 2012

Major: Environmental Geoscience

CHARACTERIZING PHYSICAL PROPERTIES AND OCEAN CURRENTS IN THE EASTERN ROSS SEA, ANTARCTICA

A Senior Scholars Thesis

by

GENEVIEVE VICTORIA GENEST

Submitted to Honors and Undergraduate Research
Texas A&M University
in partial fulfillment of the requirements for the designation as

UNDERGRADUATE RESEARCH SCHOLAR

Approved by:

Research Advisor: Alejandro H. Orsi
Associate Director, Honors and Undergraduate Research: Duncan MacKenzie

May 2012

Major: Environmental Geoscience

ABSTRACT

Characterizing the Physical Properties and Ocean Currents in the Eastern Ross Sea, Antarctica. (May 2012)

Genevieve Victoria Genest
Department of Environmental Geoscience
Texas A&M University

Research Advisor: Dr. Alejandro H. Orsi
Department of Oceanography

Rising concerns of global warming and climate change warrant further research in the seas surrounding the Antarctic continent. The eastern Ross Sea is an ideal location to study changing properties of water masses transported by a major ocean current: the Antarctic Slope Current. Glaciers in the Amundsen Sea farther upstream have experienced increased melting over the past two decades, which contributes with anomalously large amounts of freshwater to the ASC. This enhanced melting could alter the formation of Antarctic Bottom Water in the Ross Sea and elsewhere along the Antarctic continental margins. Sparse observations exist in the eastern Ross Sea, and this project characterizes the physical properties and variability of water masses present in the Little America Trough. Ice Shelf Water outflows are detected in the upper levels of the Eastern Ross Sea, and a strong north flowing current is observed in the summer suggesting the presence of a seasonal current that passes through this region. The warming and freshening indicated by previous studies is verified.

DEDICATION

To my mother, Jordan, and my father, Michael, for their constant encouragement and love that has motivated and supported me throughout my academic career.

ACKNOWLEDGMENTS

I wish to express my immense gratitude to Dr. Alejandro H. Orsi for his patience and support throughout the process of developing this project and writing this thesis. I learned a lot about Oceanography over the past few months and have gained a greater understanding of what it means to be a scientist. I also owe thanks to Chrissy Wiederwohl and Yongsun Kim for their kindness and advice during the weeks in which I was being trained in MATLAB and learning the ropes of the office.

NOMENCLATURE

AABW	Antarctic Bottom Water
ACC	Antarctic Circumpolar Current
ASC	Antarctic Slope Current
ASF	Antarctic Slope Front
AASW	Antarctic Surface Water
CTD	Conductivity-Temperature-Depth
CDW	Circumpolar Deep Water
ERS	Eastern Ross Sea
LAT	Little America Trough
MOC	Meridional Overturning Circulation
NSF	National Science Foundation
RIS	Ross Ice Shelf
SAM	Southern Annular Mode
SBE	Sea-Bird Electronics
TCP	Temperature-Conductivity-Pressure
THC	Thermohaline Circulation
UVTCP	U and V velocity, Temperature, Conductivity, Pressure
WOCE	World Ocean Circulation Experiment

TABLE OF CONTENTS

Page

CHAPTER Page

LIST OF FIGURES

LIST OF TABLES

CHAPTER I

INTRODUCTION

While the Weddell, Adelie, Amundsen and western Ross seas of Antarctica have been the subject of extensive study; the eastern Ross Sea (ERS) remains fairly unexplored. The Ross Sea plays an important role in the circulation of deep water in the Southern Ocean as it is the location where dense Antarctic Bottom Water (AABW) is formed and then introduced into the Antarctic Circumpolar Current (ACC) by the Ross Gyre. Therefore, the Ross Sea is a vital component of the Meridional Overturning Circulation (MOC). The Ross Ice Shelf (RIS) supplies fresh water to the Ross Sea, which holds significant implications for global climate change. The melting of Antarctic ice shelves affects global sea level rise. In recent years, studies of climate change have focused on the Southern Ocean with a rising interest in the eastern Ross Sea [*Jacobs and Giulivi, 2010; Kwok 2005; Thompson and Solomon, 2002; Gille, 2002*].

Recent hydrographic data provides a new characterization of the physical properties of water mass and cross-shelf transport at the Little America Trough (LAT) in the ERS (Figure 1). This Thesis also includes illustrations of the observed temporal and spatial variability in local water masses, statistical analysis of their physical properties and the influence of inshore transport on basal melting of the eastern RIS.

This thesis follows the style of *Journal of Geophysical Research.*

The meridional overturning circulation (MOC)

The mechanical process by which water masses are cycled throughout the ocean is known as MOC. Coastal upwelling brings deep waters to the surface where currents direct these masses towards the poles. As the water masses cool in higher latitudes, their density increases causing them to sink. In Antarctica, the sinking of deep water masses then contributes to the formation of bottom waters that are eventually upwelled along the coastal margin or are channeled along the ocean floor to merge with the major circumpolar current [*Kuhlbrodt et al., 2007*].

Along the coastal margin of the Ross Sea, a series of localized cross-shelf cyclonic circulations are generated by the presence of troughs. These cells allow inflow of warm oceanic water across the shelf break [*Orsi, 2009*]. Data used in this Thesis were collected at an ideal location to studying this warm oceanic inflow to the Ross Sea by the southern limb of the Ross Gyre. The LAT troughs act as corridors in which on-shelf transport of relatively warm oceanic waters and off-shelf transport of extremely cold waters takes place, thus an active area of shelf-deep ocean exchange.

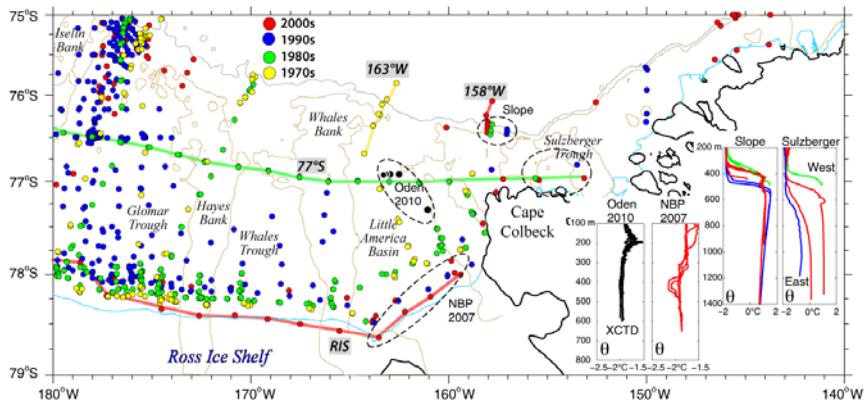

Fig. 1. Map of available CTD stations in the ERS colored by decades. Thick lines show sections in Fig. 3. The gray (tan) line is the 1500-m (500-m) isobath. Profiles of potential temperature (°C) for selected CTD/XCTD stations.

The Southern Ocean

The Southern Ocean includes the ACC and multiple weaker cyclonic circulations farther to the south, as well as those found over the continental shelf. This ocean extends from the Subtropical Front to the coast of the Antarctic continent. Along the Antarctic continental margin deep waters masses are formed, modified and then dispersed into the global ocean circulation. This ventilation of the deep ocean makes the Southern Ocean an ideal site for climate change study [*Whitworth et al., 1998*].

The southern annular mode (SAM)

The SAM is the predominant atmospheric oscillation found in the Southern Hemisphere. The strength of this mode is measured by differentiations in surface pressure at specific locations in the Southern Hemisphere [*Jacobs and Giulivi, 2010*]. When the SAM is positive, the strengthening of westerly winds amplifies upwelling along the Antarctic

coastline [*Thomspon, 2002*]. In recent years a trend of high-index polarity in the oscillations of the SAM correlates to warming in the Southern Ocean [*Thompson, 2002; Meredith and Hogg, 2006*].

The Antarctic slope front (ASF)

The ASF is indicated by the large subsurface gradients of density, temperature and salinity found on the upper continental slope of Antarctica. It separates Circumpolar Deep Water (CDW) from a thickened layer of Shelf Water (SW) inshore, and in some places where shelf waters are present near the shelf break a distinctive "V" shape is also observed [*Whitworth et al., 1998*]. The gradient of the ASF creates a westward flow along the continental slope [*Orsi, 2009*].

The Antarctic circumpolar current (ACC)

The westerly winds drive the ACC, which is the dominant current of the Southern Ocean. This eastward current encircles the entire Antarctic continent, passes through the constriction of the Drake Passage and connects the three major ocean basins of the Southern Hemisphere [*Orsi et al.,* 1999]. Antarctic water masses are carried by the ACC redistribute heat and freshwater throughout the Southern Hemisphere. As a result significant mixing and entrainment of adjacent waters take place within this current.

The sub-polar ross gyre

In the Pacific sector of the Southern Ocean and poleward of the ACC, a large clockwise circulation, the Ross Gyre, transfers warm, deep water masses from the north to the eastern Ross Sea and exports bottom water back north into the ACC [*Whitworth et al.,1998*]. Variability in the ACC acts as the northern forcing agent for this exchange.

The Ross Ice Shelf (RIS)

The RIS is the largest ice sheet in the world. It isolates underlying water masses from atmospheric forcing beyond the outer edges of the shelf. In Antarctica, 40% of the sea surface is barred from atmospheric effects by ice shelves. The unique physical properties of sub-shelf water masses directly affect basal melting rates underneath the ice shelf. A study by Hellmer and Jacobs (1995) determined that the rate of basal melt in the RIS ranges from 18 to 27 cm/yr and also that the angle of the ice shelf base has a significant impact on the melting rate. Naturally, melt rates at the top of glaciers peak in the summer season when AASW temperature increases [*Assmann and Timmermann, 2005*]. Melt-water from the RIS decreases the salinity of the underlying water masses and conversely freezing increases the salinity. It is thus postulated that rising global temperatures and consequential warming of ocean currents have the potential to increase melting rates of the Antarctic ice shelves [*Jacobs et al., 1970*].

Ice shelf water (ISW)

A key component of AABW formation is the ISQ, sub-freezing point temperature at sea

level and found at just a few sites along the continental slope and shelf [*Jacobs et al., 1985; Hellmer and Jacobs, 1995*]. Vertical mixing of shelf water (SW) leads to the overturning that can reach levels deep enough to induce mixing underneath the ice shelf [*Hellmer and Jacobs, 1995*]. The interaction between High Salinity Shelf Waters (HSSW) and the ice shelf base leads to the formation of ISW underneath the RIS, which in turn feeds the outflow of a low-salinity type of AABW [*Whitworth and et al., 1998*].

Circumpolar deep water (CDW)

The most voluminous water mass in the Southern Ocean is the warm, salty CDW of the ACC. It is brought to the eastern Ross Sea by the southern limb of the Ross Gyre where it lies between Antarctic Shelf Water (AASW) and above AABW. In the ACC regime it is partitioned into upper and lower components, distinguished by an oxygen minimum and salinity maximum [*Callahan, 1972*]. CDW plays an important role in the Ross Sea, and is a component of AABW mixed near shelf break [*Whitworth et al., 1998*].

Antarctic bottom water (AABW)

The AABW is the coldest water found at the bottom of the World Ocean, and is distinguished from other bottom waters with northern origin by its greater density, i.e. greater than 28.27 kg/m^3 [*Orsi et al., 1999*]. Due to its high density, AABW is unable to traverse the sill of the Drake Passage and therefore is not circumpolar in extent like CDW. The formation of AABW occurs in sparse locations along the Antarctic shelf, one

of which is the Ross Sea contributing with about 25% of the total production of AABW [*Rintoul, 1998*]. AABW fills the deepest layer of the ocean and its northward path is strongly controlled by the bathymetry of the Southern Ocean. In the Ross Sea, AABW is formed when surface waters become more saline and sink due to their increased density. Entraining of lighter ambient waters occurs as AABW sinks down the continental slope. The resulting bottom water then travels along the ocean floor and is exported by the Ross Gyre into the flow of the ACC [*Whitworth et al., 1998*].

Change in the Ross Sea

Strengthening in the SAM as well as slight shifts in the ASF has induced changes in the water properties of masses in the Ross Sea [*Jacobs and Giulivi, 2010*]. Studies have shown a freshening of Ross Sea waters in recent decades, in relation to larger intrusion of meltwater from the Amundsen Sea ice shelves [*Thoma et al., 2008; Jacobs and Giulivi, 2010*]. Conditions in the Ross Sea can thus be used to gauge changing conditions in neighboring regions along the Antarctic margins. Identifying the sources of these changes, such as the fluxes of CDW in the Ross Sea, may reveal shifting patterns of deep ocean ventilation outside of the Ross Sea [*Jacobs and Giulivi, 2010*].

The Oden cruise of 2010

In 2010, Dr. Orsi and a team from Texas A&M University deployed two identical moorings from the Swedish icebreaker *Oden* in the LAT. Moored instruments were programmed to take measurements every 30 minutes over the course of 14 months, from

February 2010 to March 2011. An outer shelf mooring was deployed at 77.32°S, 161.07°W. It consisted of 3 Sea-Bird SBE-37 Microcats and 2 Nortek Aquadropps 3000. An identical mid-shelf mooring was deployed at 76.93°S, 163.33°W (Table 1, Figure 2).

Objectives

The physical properties of water masses in the Southern Ocean have been described reasonably well based on extensive summer. Winter data is not available throughout the Ross Sea, and minimally in the rest of the Southern Ocean. There are four objectives for this thesis which will be met using the CTD and hydrographic data collected by Dr. Orsi and his team *during the past two years*: I) improve the description of water masses physical properties in the eastern Ross Sea; II) determine the observed current structure; III) describe the temporal variability in the local circulation; and IV) determine the extent to which net inshore transport at the outer shelf influences basal melting at the eastern segment of the RIS. Results, analyses and characterizations presented by this Thesis will supplement previous work and provide a framework for future studies of climate variability to warrant a clearer and complete understanding of this region's adjustment to climate change.

Table 1. Specifications on the instruments attached to each mooring line.

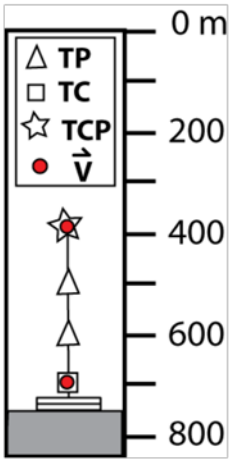

Fig. 2: Mooring schematic displaying the structure of the two mooring lines. Each mooring was equipped with 3 SBE-37 microcats and two Nortek Aquadopp-3000 current meters (top and bottom).

M1		
-77.32°	**-161.07°W**	**650m**
MCat (SBE-37)	240m	TCP
CM (AQD-3000)	241m	UVTCP
MCat (SBE-37)	435m	TCP
MCat (SBE-37)	643m	TCP
CM (AQD-3000)	643m	UVTCP

M2		
-76.94°S	**-163.33°W**	**600**
CM (AQD-3000)	185m	UVTCP
MCat (SBE-37)	187m	TCP
MCat (SBE-37)	383m	TCP
MCat (SBE-37)	590m	TCP
CM (AQD-3000)	590m	UVTCP

CHAPTER II

METHODS

Mooring array

The two ERS moorings were deployed in February 2010 and retrieved in March 2011. Mooring A was located at a depth of 650 m below the surface and Mooring B at 600 m. Each mooring line consisted of 5 instruments that "monitored" directly seawater temperature, salinity, pressure and currents direction and velocity. All of the instruments were successfully recovered in good condition. The instruments provided the required data to adequately describe the oceanographic conditions of this easternmost entry region to the Ross Sea. The specific positioning of the moored instruments covered the vertical range in which the expected source and outflow waters from the cavity of the RIS.

The data turnout of the moorings exceeded ninety percent. Thus, newly measured time series analyzed here are unique to the better understand of basal melting in the World's largest marine ice shelf, its grounding line stability, and the property exchange across its front that reflect the year-long local air-sea-ice interactions.

Instruments and time series

Time series of CDT and currents for this project were recorded with instruments attached to two moorings deployed in the LAT. Each of the moorings was equipped with three Sea-Bird SBE-37 microCATS located at depths of 240 m, 440 m and 640 m and

two Nortek Aquadropps 3000, located at 240 m and 640 m. The three microcats on Mooring B were attached at 187 m, 387 m and 587 m, and also paired with two Aquadropps at the top and bottom levels.

All instruments recorded data at 30-minute intervals for a period of 14 months. In this study pressure and temperature measurements from the SBE-37 microCAT sensors will be used for analysis of pressure measurements since they are more accurate than those provided by the Nortek Aquadropps (Figure 3). Only one of the 10 instruments experienced loss of data. The 241 m Nortek Aquadropp on Mooring line A stopped taking measurements on September 16, 2010. This did not dramatically impact our ability to interpret the rest of the data.

Quality control and data reduction

The principal tool for analysis of the time series data acquired from the ten instruments was R2010b "version" of MATLAB. Raw data output from all instruments were converted to a working file format compatible with MATLAB routines used in their reduction, quality control and analysis. Sea-Bird Electronics carried out the post-deployment calibration of all sensors. Upon receiving the calibrations, we removed segments of the record prior to the mooring settlement at the ocean floor and recovery at their release. Corrections to account for sensors drift during the deployment period were applied to the raw data using available MATLAB scripts.

To process the post-calibrated data, a script designed to remove spikes was run. Anomalous data points with values exceeding three standard deviations from the third order polynomial fit of the data (time series) were marked as a “spike” uncharacteristic of the time series. This data reduction process was applied to all measured variables concurrently, i.e. temperature, conductivity, pressure and velocity, from a particular instrument to better identify the correlation between spikes. The time series were processed in a series of 4-day windows and each data point flagged by the program as a potential spike was humanly by eye to verify its validity, i.e. to confirm or reject its being an actual spike.

The filling in of potential small to medium size gaps in the time series is normally conducted using different methods. A linear 17-point interpolation method is applied to any gap shorter than six hours long, whereas longer gaps are dealt with by single spectrum analysis. Remarkably, there were absolutely no gaps in any of the time series.

Since the microcats and aquadropps did not measure exactly the same properties, the program derived the missing values by interpolating from the neighboring instruments using the Seawater Toolbox version 3.3. After these quality control steps are completed, each time series was run through a 40-hour low pass filter and a 30-day filter, which are necessary to investigate features with different

temporal scales.

Statistics

Basic statistical analysis of the time series data is performed next. Calculated record-length mean properties and currents and the statistics of their variability are summarized here. This information is used to compare measured characteristics at different levels, and to contrast them with those derived from existing hydrographic station data. This comparison will help identify potential inter-annual changes in the region's oceanographic conditions. The overall objective of this data analysis is to characterize the mean variability, both spatial and temporal, properties in the eastern Ross Sea.

Long-term measurements from the Eastern Ross Sea mooring array will be used to characterize the mean and dominant scales of variability associated with the oceanic inflow to the Ross Sea long the eastern flank of the Little America Trough. In addition, they will provide a time-domain context for interpreting the shipboard CTD/LADCP data from the 2011 S4P CLIVAR hydrographic cruise on the RVI N.B. Palmer [*Orsi, 2009*].

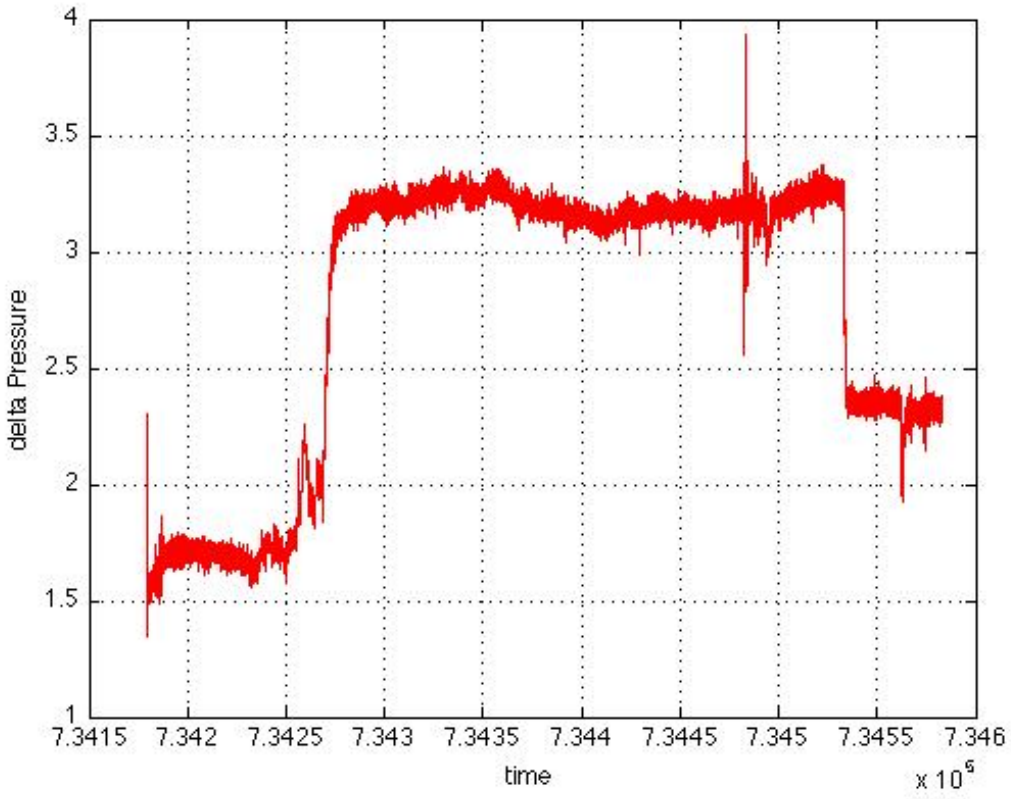

Fig. 3. The pressure difference between paired instruments. Microcat (Mooring 2 at 185 m) and Nortek Aquadropp-3000 (Mooring 2 at 187 m).

CHAPTER III

RESULTS

The following sections provide a preliminary analysis and description of the physical properties and currents measured by the ten instruments on the two 1-year moorings deployed from the *Oden* in the eastern Ross Sea between the years of 2010-2011. By running the raw data through a 40-hour low pass filter, the tidal components of the time series were removed. It is the de-tided data set with which all the statistics and analysis has been calculated and conducted. Year-long records for each instrument were examined as well as hydrographic data in the form of contoured vertical sections from the stations at and near the sites of these two moorings.

The observed vertical distributions are complemented by the graphical analysis of T-S scatterplots for each instrument and their correlating mean statistics. The data collected for this project is then compared to a number of other records collected by similar studies over the past several decades in the immediately surrounding region explored in this project. The collective data sets are displayed in surface contour maps.

Time series

Potential temperature was then calculated for the SBE-37 sensors using a script that corrects for the pressure effect on temperature. These plots are shown in Figure 4 for M1 and M2. Figure 5 displays the time-series for salinity, which was derived from conductivity measurements, and neutral density. The gray lines indicate the top instrument microcats at their mean depths; the orange lines represent the middle microcats; and the purple lines indicate the bottom instruments. Figure 6 depicts the time series for neutral density. The time series for the east/west u and north/south v velocity components for the entire record are shown in Figures 7 and 8 for M1 for M2. The 241 m current meter on M1 failed in late September for unknown reasons and therefore the record for the last half of its time series is incomplete.

Spectra analysis

Spectral analysis partitions the variance as a function of frequency and therefore is a useful tool for identifying the tidal components of time series data [*Talley et al., 2010*]. In Figure 9, the power spectral analysis for the 643 m SBE-37 sensor on M1 is

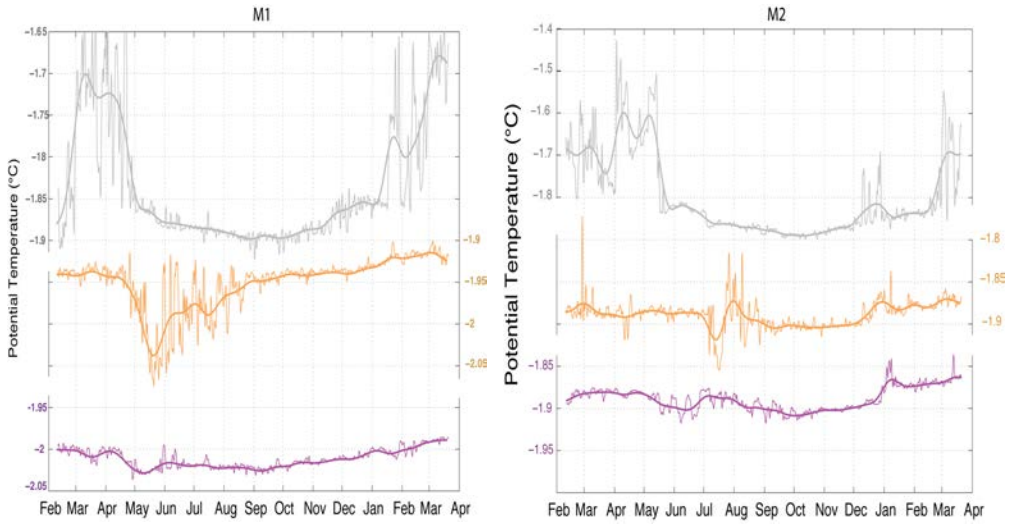

Fig. 4. Time series for record-length Potential Temperature. M1 (left) and M2 (right) with 40-hour low pass and 30-day low pass filters.

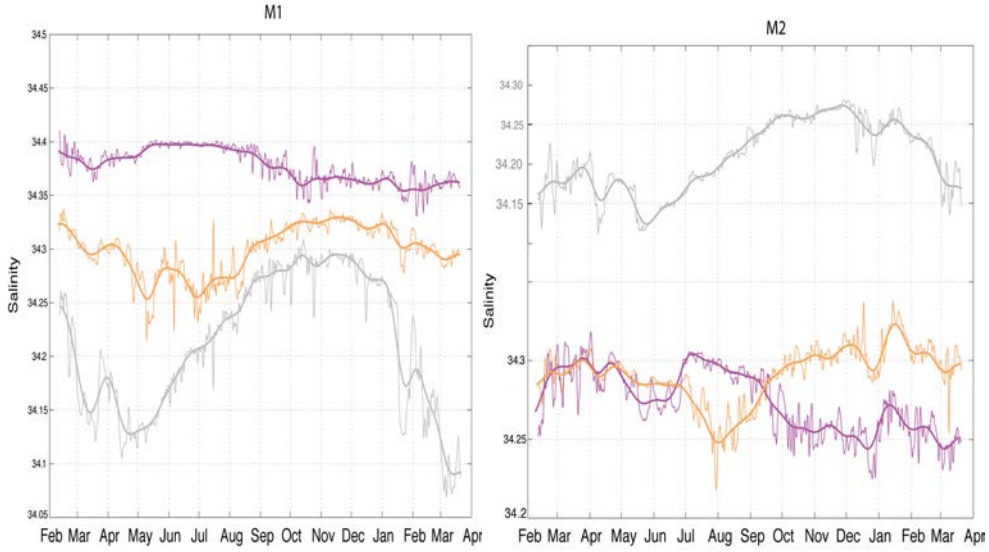

Fig. 5. Time series for record-length Salinity. M1 (left) and M2 (right) with a 40-hour low pass and 30-day low pass.

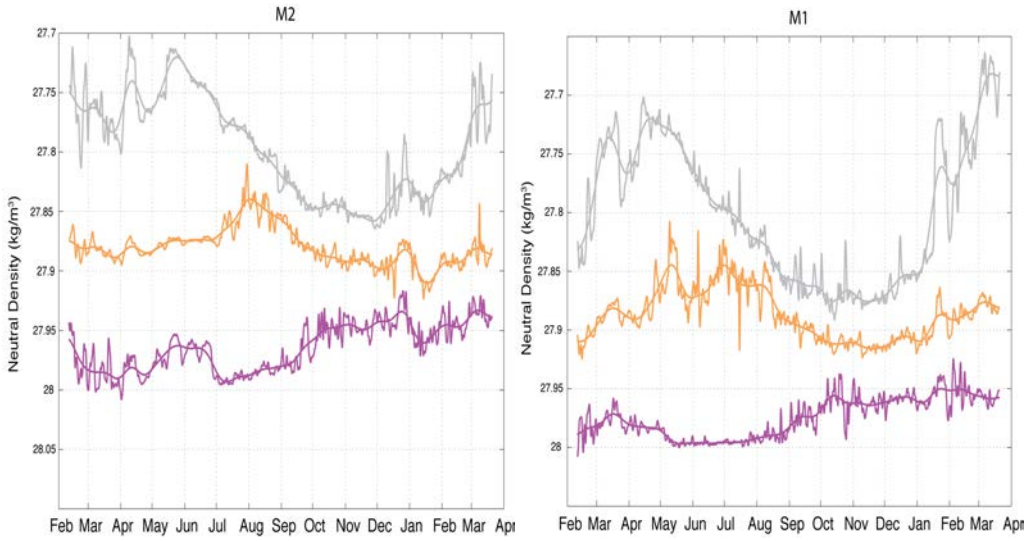

Fig. 6. Time series for record-length Neutral Density. M1 (left) and M2 (right) with a 40-hour low pass and 30-day low pass.

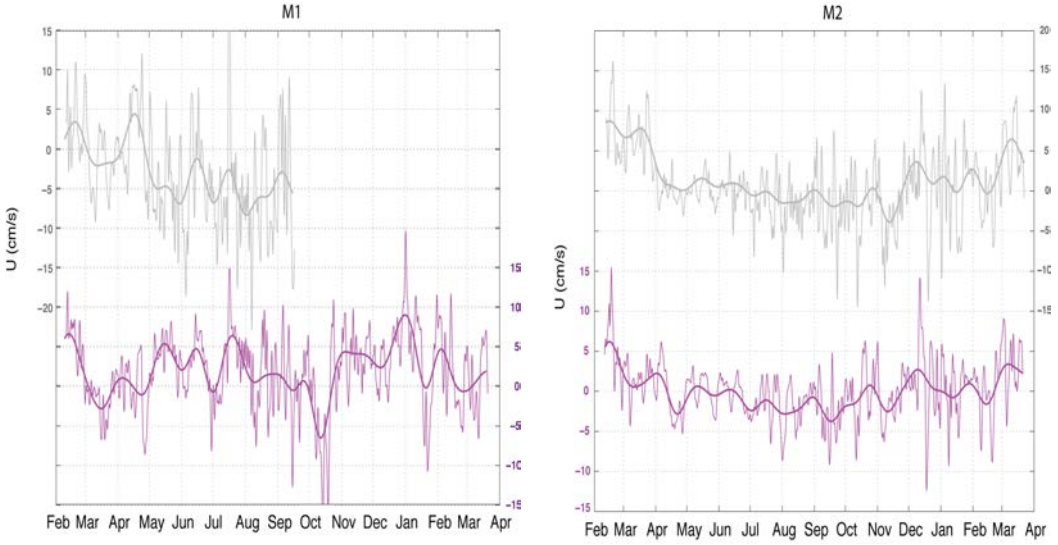

Fig. 7. Time series for record-length U velocity component. M1 (left) and M2 (left) with a 40-hour low pass and a 30-day low pass.

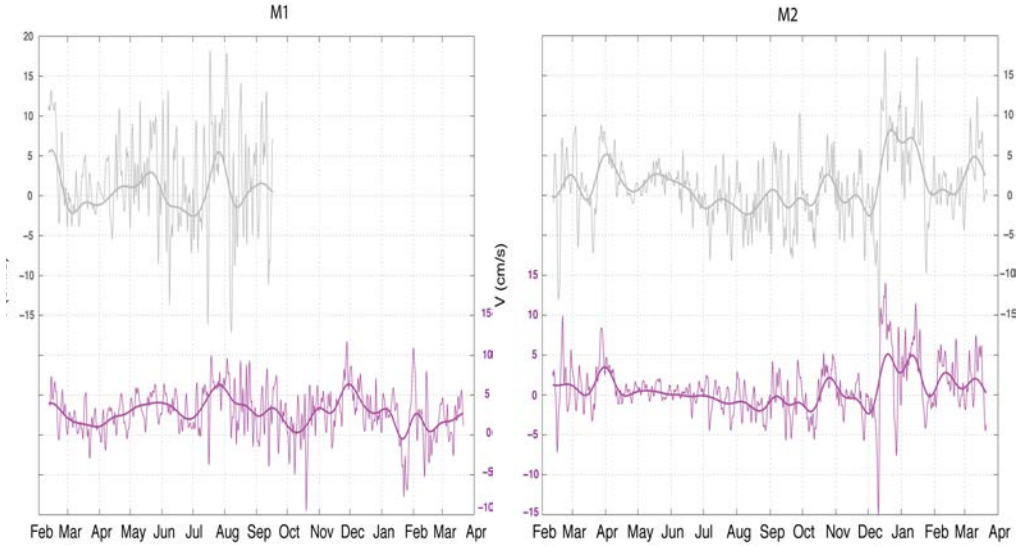

Fig. 8. Time series for record-length V velocity component. M1 (left) and M2 (right) with a 40-hour low pass and a 30-day low pass.

shown and is representative of the entire set of time series for all the instruments. It is easy to identify two bands of high-energy frequencies, the highest of which is the diurnal constituents, labeled as O1 and K1 and the second is the semidiurnal constituent, labeled as M2.

Temperature-salinity trends

Figures 10 and 11 illustrate the relationship between temperature and salinity for the SBE-37 sensors on both moorings after the data were run through a 40-hour low pass filter. The correlation between these two properties illustrates that the same water masses were monitored at both locations. The gray scatter points represent the top instruments on both moorings; the orange scatter points represent the middle instruments, and the purple scatter points indicate the bottom instruments. The blue and red lines show the measurements recorded at station 74 (blue) near M2 and station 69 (red) near M1. The small shapes indicate the record-length means for each instrument.

Table 2. Record-length means for M1 and M2. Properties shown are potential temperature, salinity, neutral density, u-velocity component and v-velocity component.

Record-length mean and standard deviation of 40-hour low pass filtered data.

		Θ (°C)		Sal		γ(kgm-3)		u (cm/s)		v(cm/s)	
M1											
SBE-37	**240m**	-1.837	0.0781	34.2122	0.0635	27.8008	0.596	--		--	
AQD-3000	**241m**	--		--		--		-3.0649	7.4	1.6142	6.4688
SBE-37	**435m**	-1.911	0.0346	34.2985	0.0243	27.8867	0.0227	--		--	
SBE-37	**643m**	-1.895	0.0113	34.378	0.0164	27.9745	0.0173	--		--	
AQD-3000	**643m**	--		--		--		1.8913	5.2379	2.6172	3.2815
M2											
SBE-37	**187m**	-1.8003	0.0907	34.2084	0.0452	27.7964	0.0431	--		--	
AQD-3000	**185m**	--		--		--		0.03073	5.0323	1.1181	4.943
SBE-37	**383m**	-1.8886	0.0192	34.292	0.0162	27.88	0.0166	--		--	
SBE-37	**590m**	-1.8883	0.143	34.3722	0.0211	27.9645	0.0206	--		--	
AQD-3000	**590m**	--		--		--		0.0905	2.0941	0.7457	3.7466

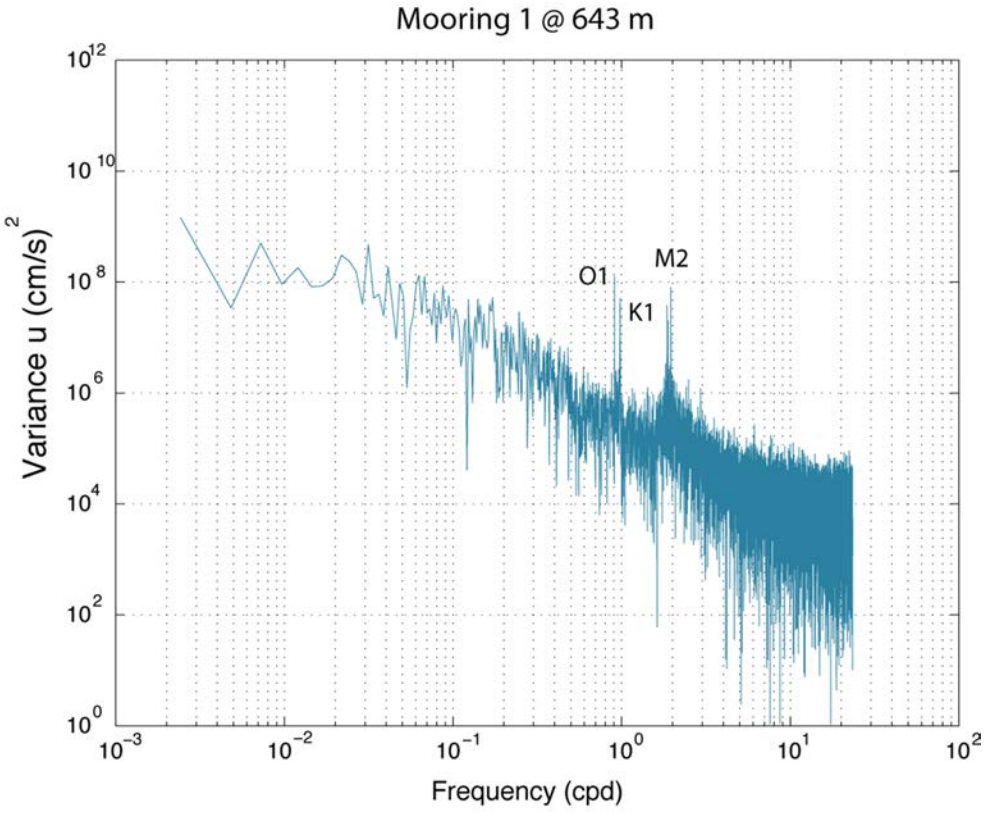

Fig. 9. Power spectra of the 643 m instrument on M1. O1 and K1 label the diurnal tidal component and M2 indicates the semidiurnal component.

Physical and current properties

In Table 2 the record-length means for the water mass properties and velocity components for each instrument on both moorings are presented. The Nortek Aquadopps-3000 did not record salinity measurements and therefore there are no salinity measurements for the four current meters. Comparison of the moorings shows significant similarity between mean values. This becomes evident by looking at the mean TS relationships for each instrument, which can be observed in Figures 10 and 11. The freezing line is drawn on the figures as the slightly sloping dashed line. Data from all six SBE-37 sensors dip below the freezing temperature, which suggests they all experienced the passing of a common water mass for a period of time, possibly an outflow of ISW. Average densities center around 27.8 kg m^{-3} and salinity values have an average of 34.3, which is characteristic of AASW that lies above CDW and has a lower bound of 28.00 kg m^{-3} [*Orsi, 2009*]. The maximum density (~28.05 kg m^{-3}) and salinity (~34.40) were measured by the bottom instrument on M1 at 643 meters below the surface.

The warmest water temperatures (-1.6 °C) were measured by the top instrument on M2 (farther from the ice shelf) located at 187 meters below the surface. The coldest recorded temperature (-2.05 °C) was measured by the SBE-37 sensor lying at 435 m on M1.

In general, the mean speeds for all four current meters is relatively consistent falling in the range of 5-15 cm/s. Mean current velocities for both moorings show a predominant northward flow at the sub-surface as well as along the bottom. The strongest current speeds are observed in the beginning of the 2011 summer season in the top instrument on M1 (~30 cm/s). This captures the flow of water masses away from the ice shelf during the summer melting season. However, the current meters on M2 exhibit a prolonged southward flow during the winter season. The topographical orientation of the LAT in the Ross Sea serves to direct these currents in the north-south direction.

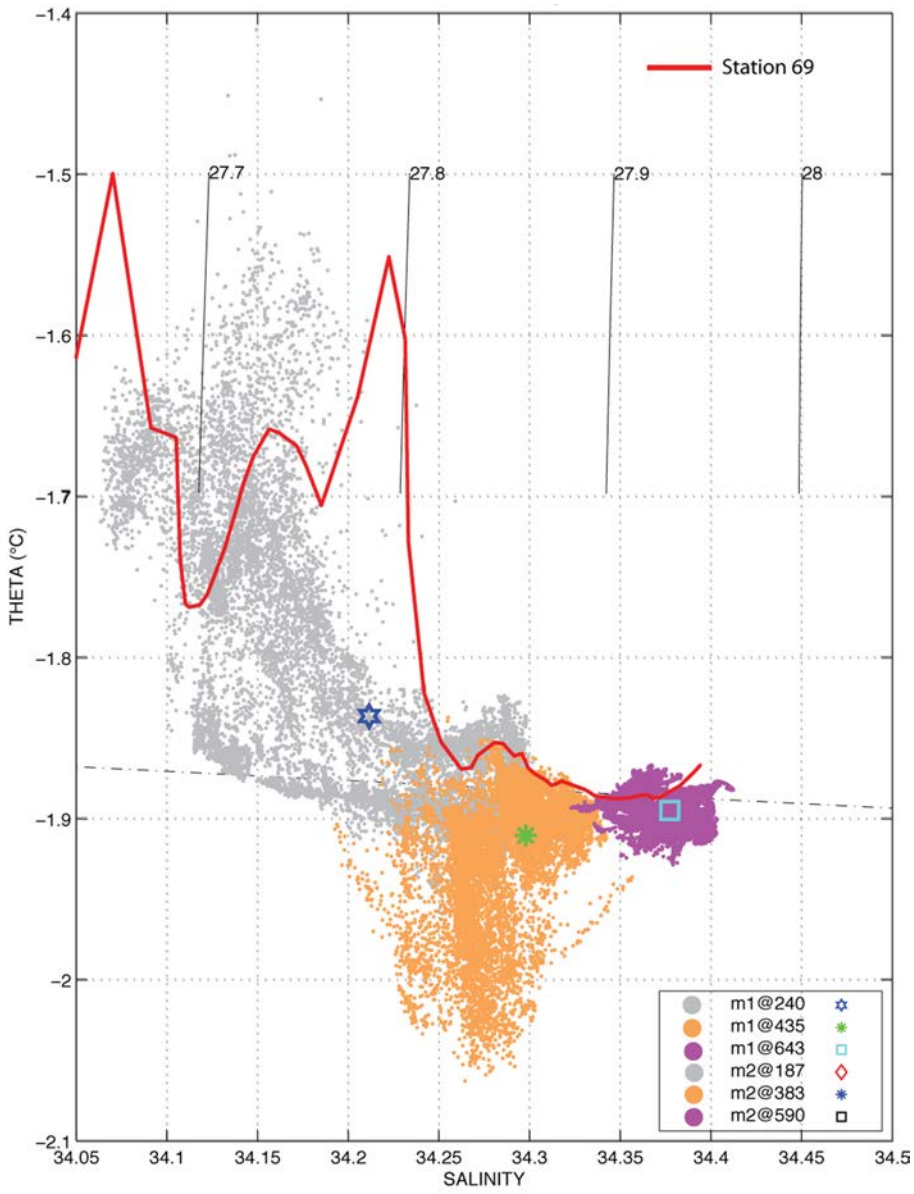

Fig. 10. The temperature-salinity scatter plot for M1. The red line indicates the values measured at station 69 along section 1. The three symbols represent the record-length means for each instrument.

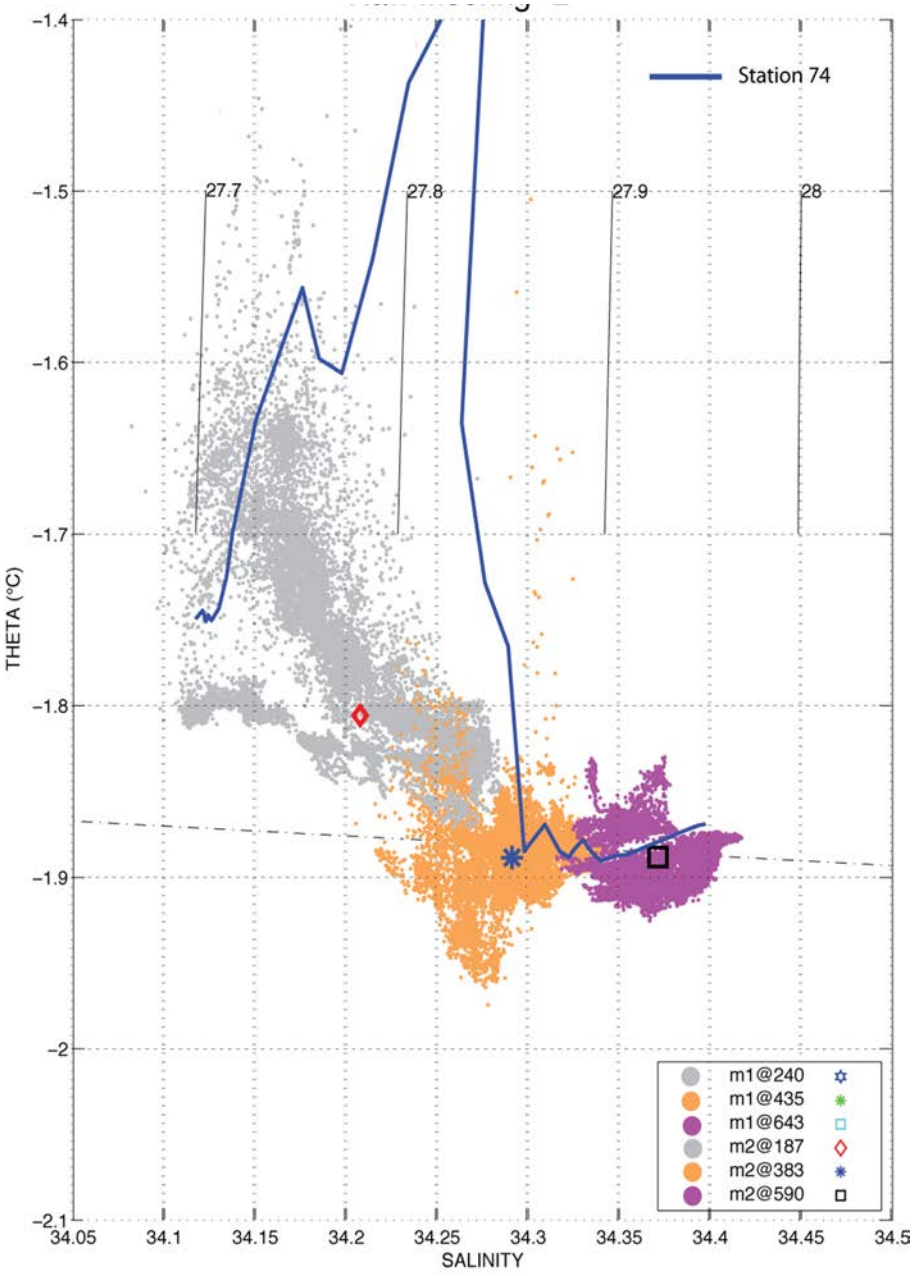

Fig. 11. The temperature-salinity scatter plot for M2. The blue line represents the measurements made at station 74 along section 2. The symbols represent the record-

Vertical sections

The vertical sections of properties along two hydrographic sections spanning the mooring sites are presented in Figures 12 through 16. They show the potential temperature, salinity, neutral density, oxygen, and speed component fields. Mooring 1 was deployed at the site of station 69 on section 1 and Mooring 2 was deployed near station 74 along section 2. These stations were sampled close to the time when the moorings were deployed in February 2010 and therefore provide a glimpse of the vertical distribution of properties at a single moment in time.

The stars on the sections signify the location of each instrument on M1 and M2. The empty stars indicate the SBE-37 microcats and the stars with internal pentagons indicate the SBE-37 microcat-Nortek Aquadopp-3000 pairs.

In the M1 section, which was farther away from the RIS, potential temperature, salinity and density all exhibit similar vertical patterns such as the steeping of the contours moving from left to right towards the eastern edge of the trough. M2 displays an interesting plume of warm water intruding from the east into the trough near the location of the 435 m sensor.

Comparison to hydrographic data from sections sampled on other cruises could provide insight into some of the unique physical features captured by these sections. This will be done in the next chapter.

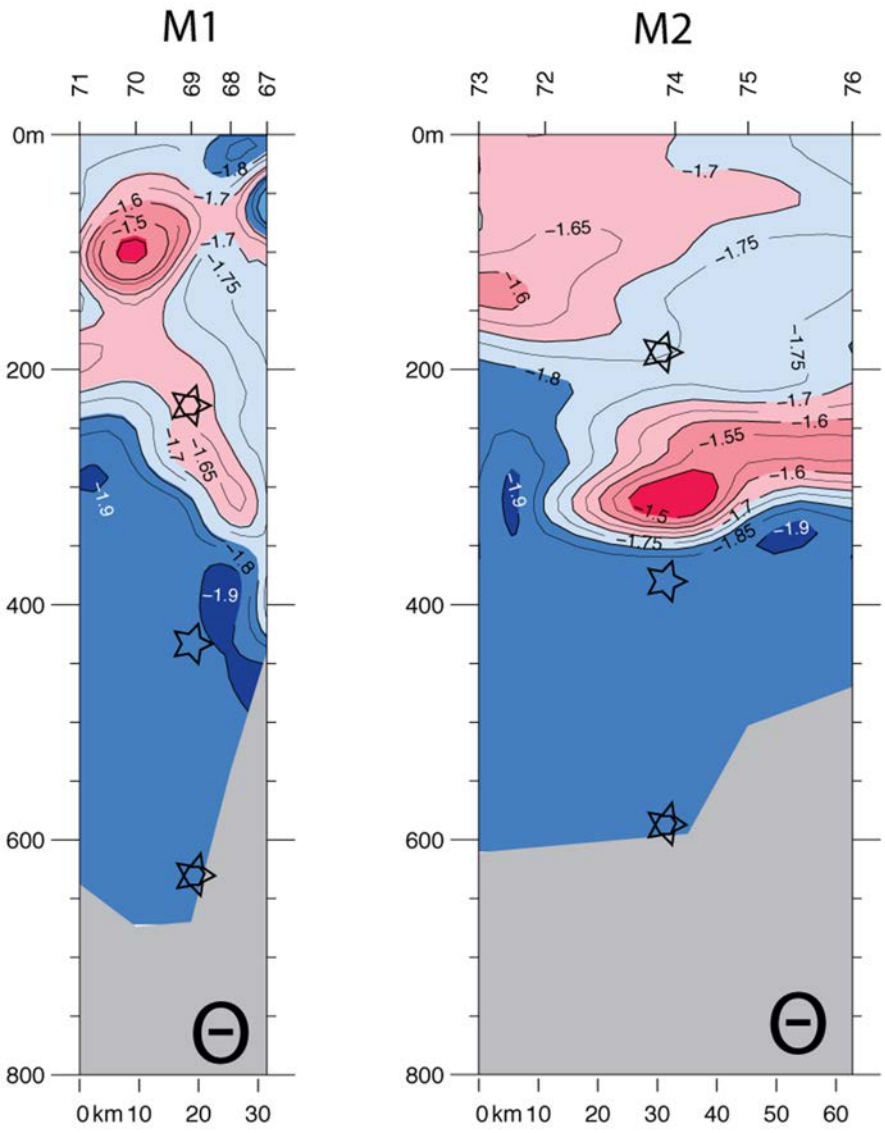

Fig. 12. Vertical sections of Potential Temperature. Section 1 (left) and section 2 (right).

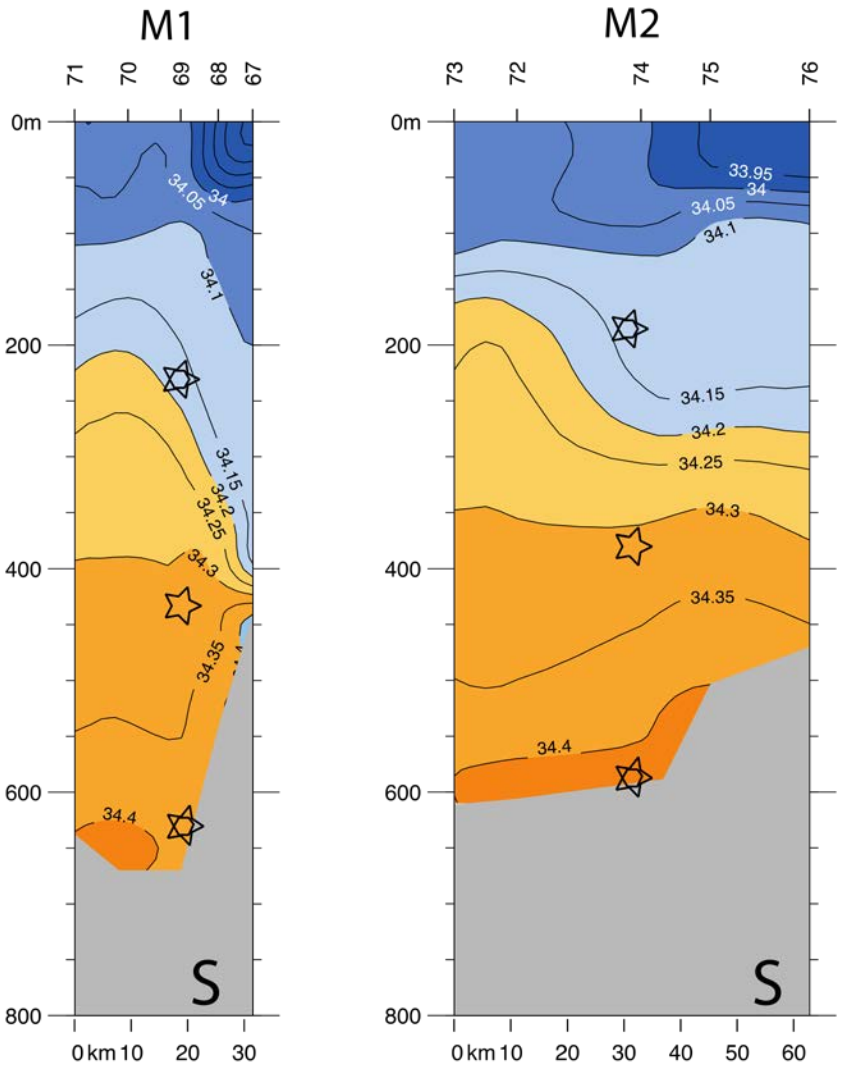

Fig. 13. Vertical sections of Salinity. Section 1 (left) and section 2 (right).

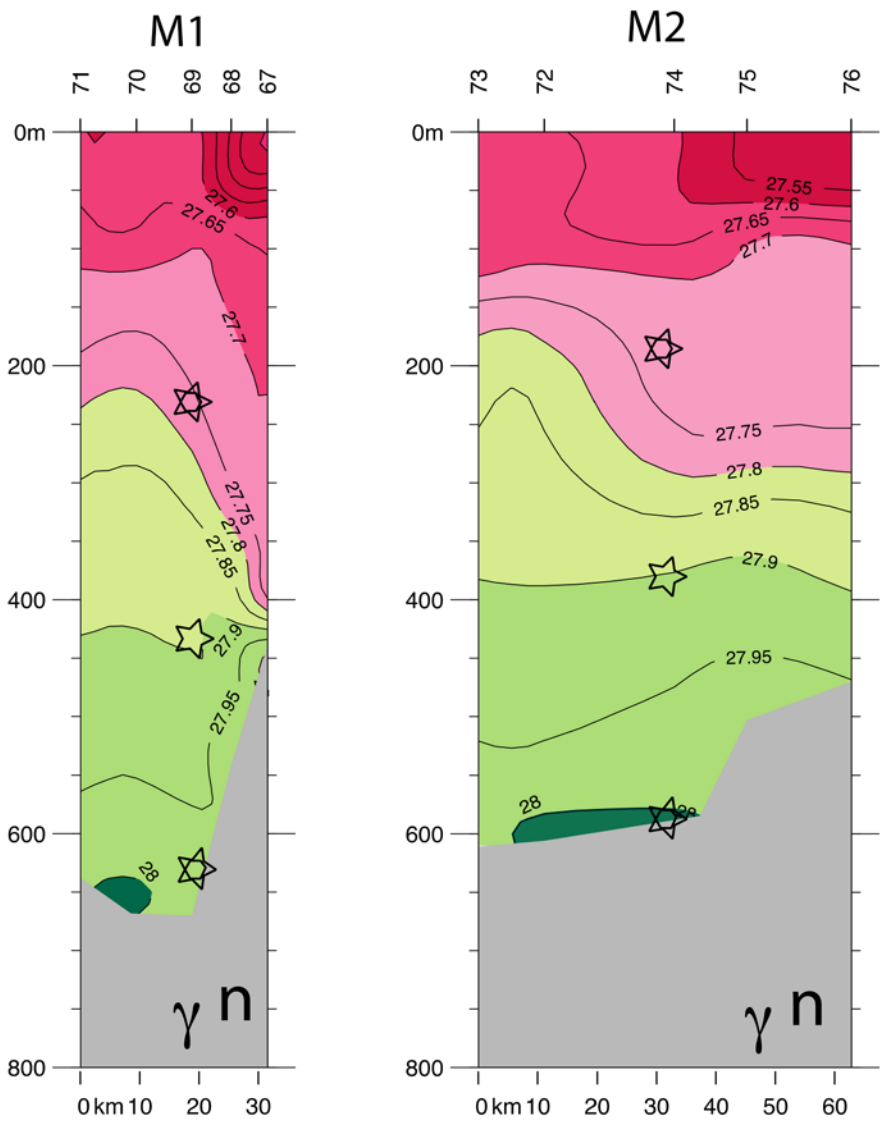

Fig. 14. Vertical sections of Neutral Density. Sections 1 (left) and section 2 (right).

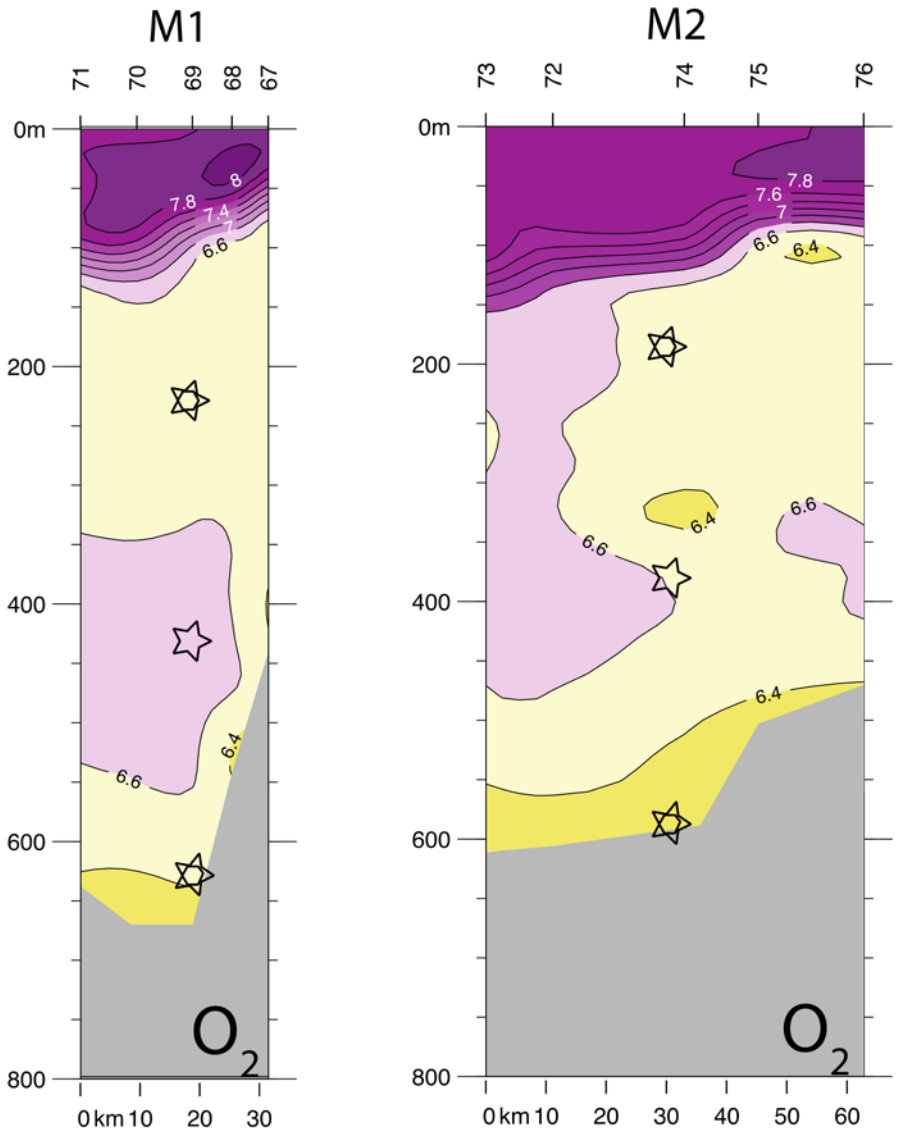

Fig. 15. Vertical sections of Oxygen. Sections 1 (left) and section 2 (right).

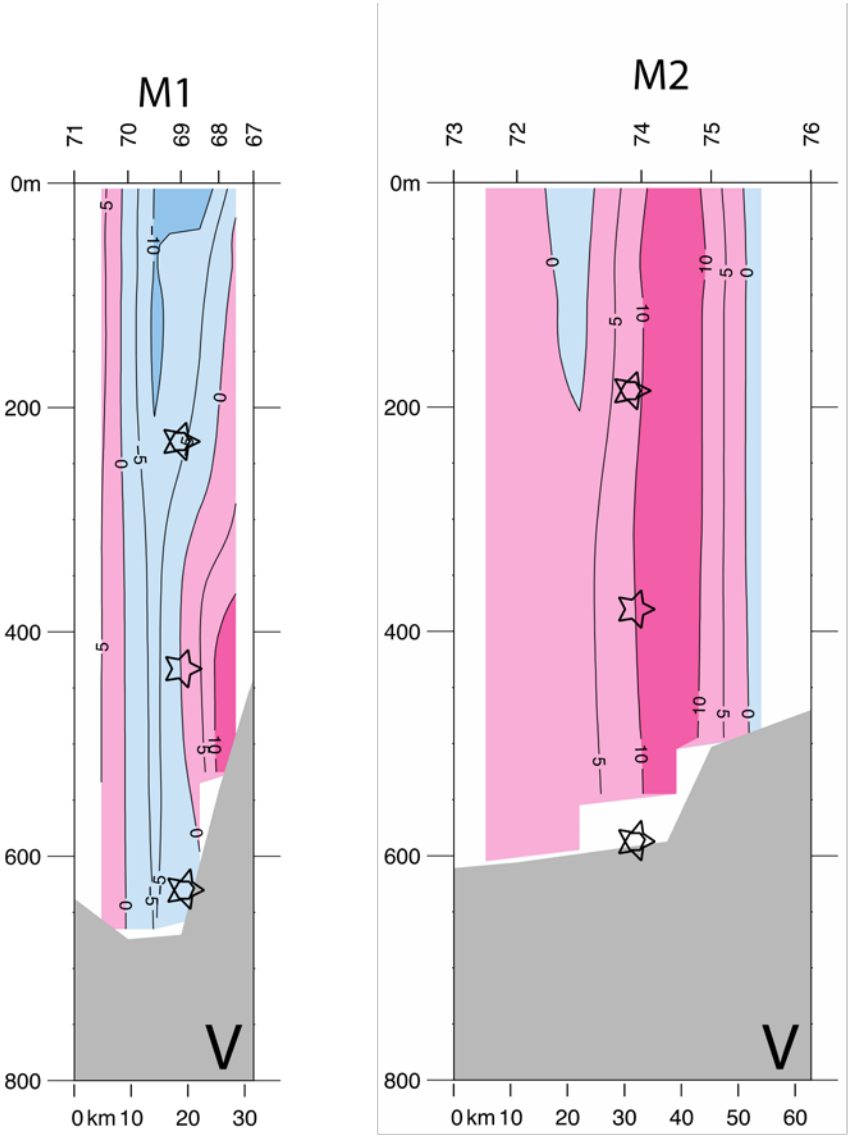

Fig. 16. Vertical sections for the adjusted and detided (+North) component. Section 1 (left) and section 2 (right).

CHAPTER IV

SUMMARY AND CONCLUSION

The Antarctic Slope and Coastal Currents transport cold, low salinity surface water along the shelf that separates the Amundsen and Ross Seas. The coastal currents then bring these subsurface waters around Cape Colbeck and southward directly towards the exposed Ross Ice Shelf, guided by the bathymetry of the LAT. Through the analysis of a year-long record of physical properties and currents, this project has provided a hydrographic summary of the water masses and transport flows along the LAT in the eastern Ross Sea and is supplementary to preexisting studies of this region as well as the waters upstream towards the Amundsen Sea. The identification of outflows from the ice shelf in the winter season are represented by the strong northward flows and the presence of ice shelf water detected by the upper and mid-level instruments on the moorings.

Θ-S relationships

Comparison of the vertical structure and evolution of Θ-S characteristics at the mooring sites revealed significantly more variability than that captured by the vertical sections, such as in the two sections sampled in the LAT as displayed to the right. The waters seen in the vertical sections for P16 provide information on the characteristics of water masses before the flow west into the Ross Sea.

Stratification in the ocean occurs is an effect of density distribution both vertically and horizontally. Temperature is indicative of a number of environmental factors such as glacial and ice shelf melting, intrusions of foreign water masses, sea ice cover, and other seasonally observed patterns while salinity gives information not only about freshwater inputs and meltwater flows but also of the origins of water masses. In combination, temperature and salinity determine the density of a water mass and are the primary physical properties used to define the various water masses identified in the ocean.

The top instruments captured the seasonal Θ-S evolution of surface waters during sea-ice formation and melting, as well as the presence of near-surface waters with temperatures below the surface freezing point during the winter. This may be evidence of ice shelf water outflows reaching these depths during the transition from the summer/spring to winter seasons [*Jacobs et al., 1970*]. The middle microcat instruments show the bulk of outflowing ice upper waters is most prominent during the winter months. During the late summer to early spring season, both of the bottom instruments show the likelihood of low salinity shelf water formation.

In the late winter and early spring of the time series (September 1 to December 15), the densities for all six SBE-37 microcats show an expansion, as seen in the convergence of the instruments' measurements towards a narrow range of densities. The transition from winter to spring occurs along the freezing line and within the salinity range of 34.25 to 34.35.

The three symbols positioned on Figures 10 and 11 mark the mean temperature and salinity values for each microcat. The mean values lie in a narrow range suggesting a certain degree of homogeneity between the mooring locations and even within the water columns surrounding the moorings.

The T-S scatter plots in Figures 17 through 22 show the relationship between temperature and salinity for the three microcats on both moorings, much like figures 10 and 11 and the colors correspond to the partitioned seasons in the example time series of the temperature record for the 240 m microcat on Mooring 1. The time series were divided into three identifiable seasons, the first season is defined by combing the end of the time series from December 15 with the beginning of the time series until June 1 (together completing the extended winter season); the second is recognized as the late winter to early spring season from June 1, 2011 to September 1, 2011; and the third is the summer season from September 1 to December 15. On the scatter plots, the dots correspond to individual data points from the 40-hour low pass filtered record for a single microcat. The small subplot on each figure displays the 30-day low pass filtered data connected by colored lines to better exemplify the change in the T-S relationship over time. The winter season is marked on the scatter plots as the dark blue colored dots; the spring season is shown as the light blue dots and the summer season is displayed as the red dots.

The contour lines in the background of the plots represent neutral density and have been

included to reference the water masses captured by the record measurements. The neutral density range measured by the instruments brackets the classification of water masses between 27.7 and 28 kg m^{-3}. The majority of the measurements fall within the 27.7 and 27.9 kg m^{-3} contours characteristic of AASW. There are no intrusions of warm CDW along the slope detected in the summer data.

Time series analysis

The time series convey active ocean-ice interactions. Relatively warm subsurface waters present during the summer precede outflows of intermediate meltwater during the winter period. A persistent, weakly stratified water column is observable throughout the remainder of the year.

Table 3 presents the mean values for each of the three identified seasons. Referencing observable changes in physical properties and currents can assess the variability of water masses. The time series plots display a close correlation between measurement trends for the instruments on each mooring. The microcats exhibit signals similar to one another suggesting consistency in the variability of physical properties with depth. These relationships are apparent when visually examining the time series.

Seasonal variations are also evident in the time series and have been marked on the plots to correspond to the colors used on the T-S plots. Identifying gradual changes over a brief period of time does marking the transitions between seasons. The summer and

winter seasons are most distinctive and almost seem to merge directly into one another, but the period in which accelerated change occurs highlights the spring season. The Antarctic summer brings cooler temperatures and therefore the freezing and formation of sea ice. Therefore, the summer can be observed on the time series as the period in which salinity and temperature share an inverse relationship. Densities as well as the area of sea ice cover increase during this time.

The summer melting period is seen at the beginning and end of the time series marked by red lines, while the winter formation period is highlighted between the light blue lines. On both mooring lines, the three levels of instruments show similar trends in variability that is consistent throughout the seasons.

Table 3. Means for seasonal sections of the time series records by instrument.

*Record-length means for each instrument during the time periods indicated in the scatter plots. December 15 through March and Feb 1 through May 1 mark the winter season, while May 1 through December 15 mark the summer season.

M1		Dec 15 - Mar 30	Feb 1 - May 1, 2011	May 1 - Sep 1	Sep 1 - Dec 15
240	ptm	-1.7857	-1.7634	-1.8828	-1.8861
	sal	34.1822	34.1682	34.2024	34.2846
435	ptm	-1.8834	-1.9029	-1.9455	-1.9021
	sal	34.3049	34.3013	34.2725	34.3211
643	ptm	-1.8827	-1.8895	-1.9046	-1.901
	sal	34.3606	34.3838	34.3958	34.3688
M2					
187	ptm	-1.7998	-1.6783	-1.8154	-1.8754
	sal	34.2245	34.1759	34.1731	34.2594
383	ptm	-1.8768	-1.8848	-1.8898	-1.9011
	sal	34.3055	34.2947	34.2747	34.2976
590	ptm	-1.872	-1.882	-1.8929	-1.9025
	sal	34.3524	34.3909	34.3854	34.3607

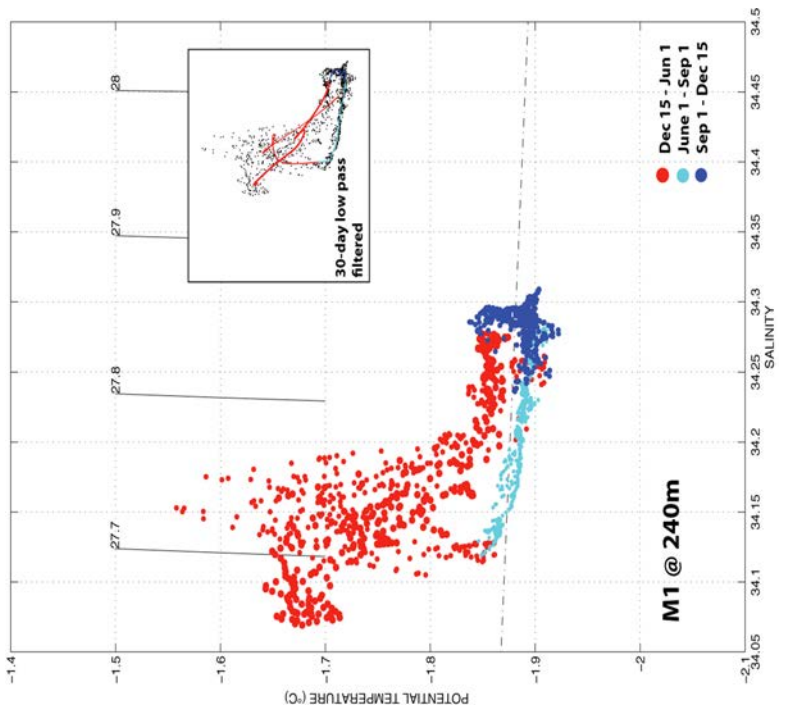

Fig. 18. The scatter plot of potential temperature versus salinity on M1 @ 240. 40-hour low pass filtered data from the top instrument on M1.

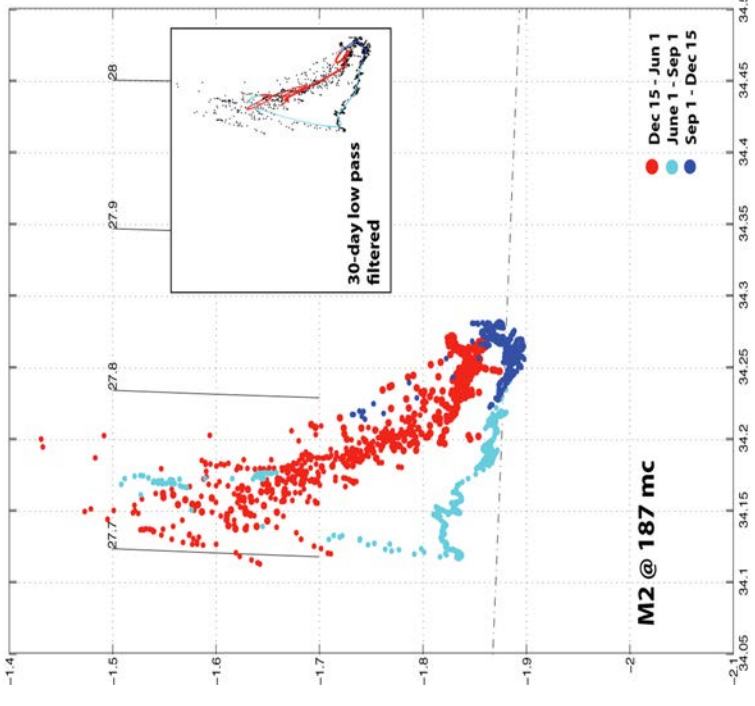

Fig. 17. The scatter plot of potential temperature versus salinity on M2 @ 187. 40-hour low pass filtered data for the top microcat on M2

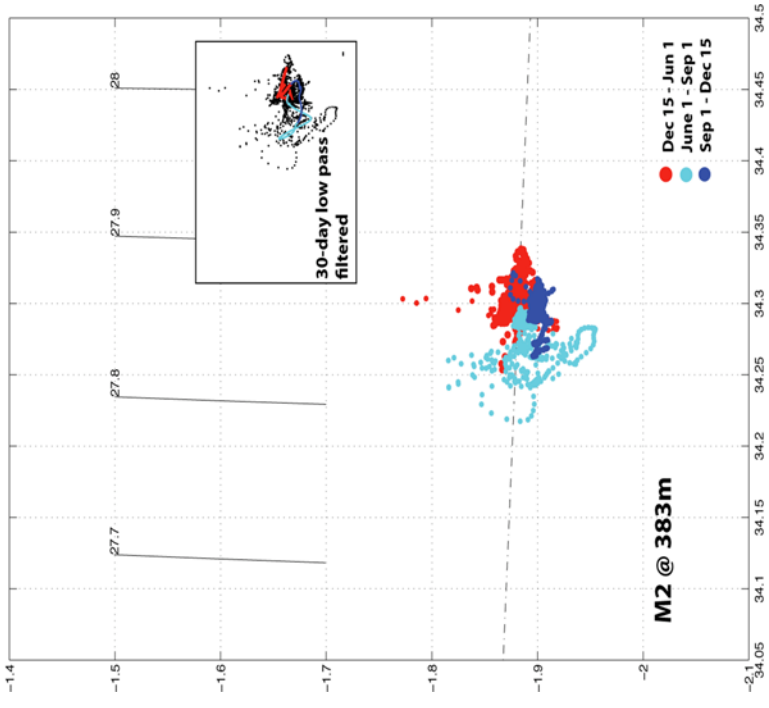

Fig. 19. The scatter plot of potential temperature versus salinity on M2 @ 387. 40-hour low pass filtered data from the middle microcat on M2.

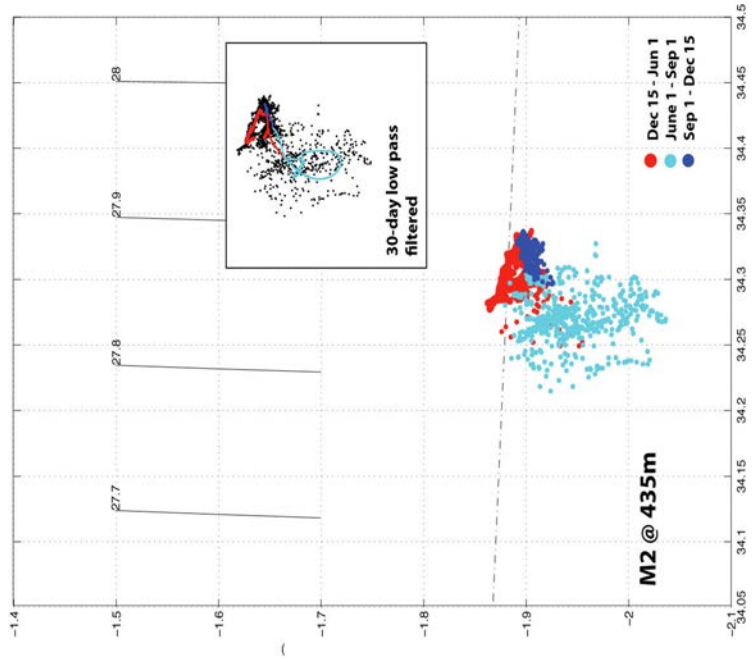

Fig. 20. The scatter plot of potential temperature versus salinity on M1 @ 435. 40-hour low pass filtered data fro the middle microcat on M1.

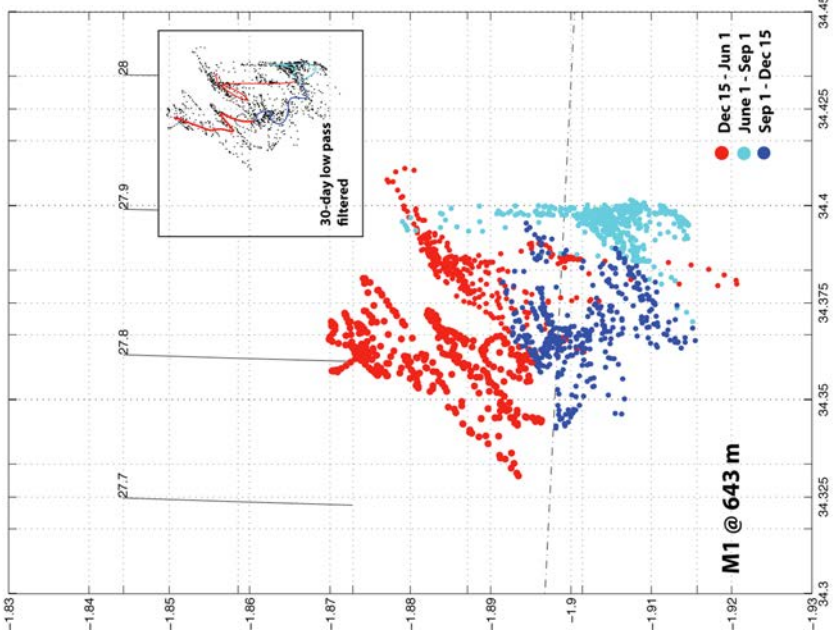

Fig. 22. The scatter plot of potential temperature versus salinity on M1 @ 643. 40-hour low pass filtered data fro the bottom microcat on M1.

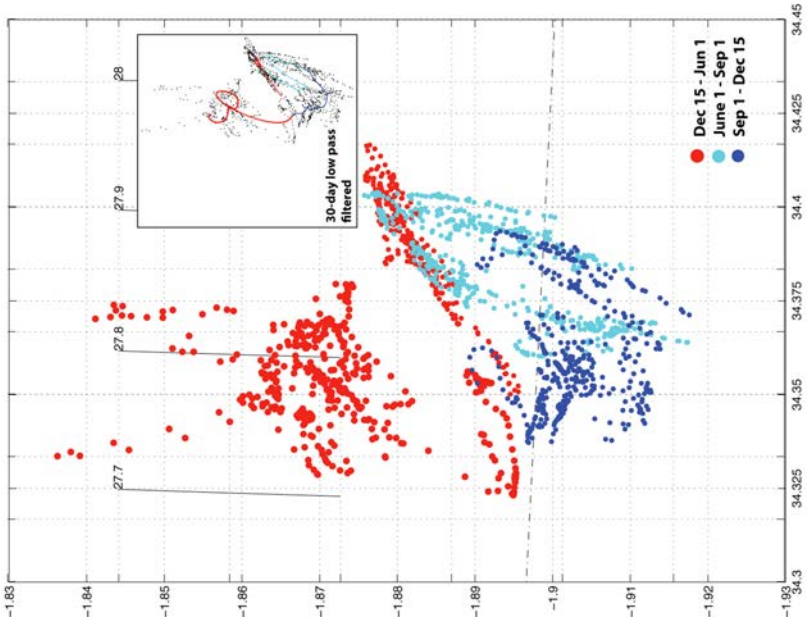

Fig. 21. The scatter plot of potential temperature versus salinity on M2 @ 590. 40-hour low pass filtered data fro the bottom microcat on M2.

Sea ice cover

Figure 23 shows a time series of sea-ice area in the Ross Sea showing the annual signal of sea ice cover over the course of ten years. Each data point represents a monthly average. The dips in the time series correlate to the summer months where melting rates increase. Figure 26 shows an image capture of the region on February 21, 2011 towards the end of the record; Figure 24 captures sea ice cover on March 1, 2011 and Figure 24 shows ice cover on March 17, 2011. Just by glancing at the three figures in succession, it is easy to see the dramatic change in sea ice cover over a month's time. The ice slowly extends from the continent out into the sea and in Figure 25 M1 appears to be in the midst of a 50-80% sea ice cover. These dates relate to the very end of the time series records.

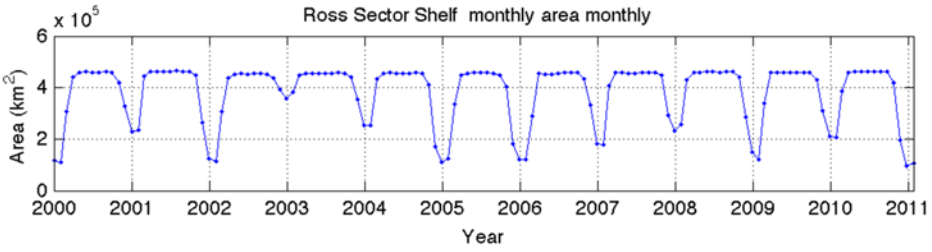

Fig. 23. Sea ice extent on the Ross Sea Shelf.

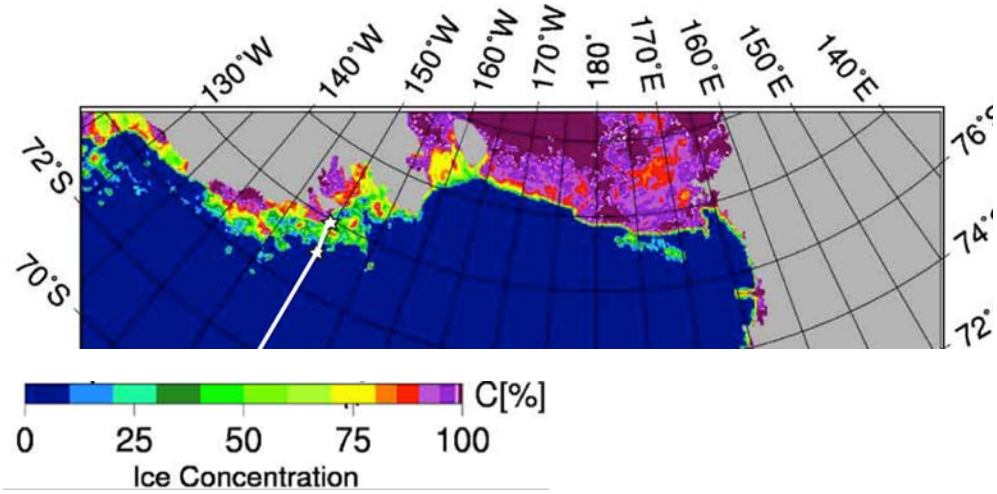

Fig. 24. Sea ice cover on March 1, 2011

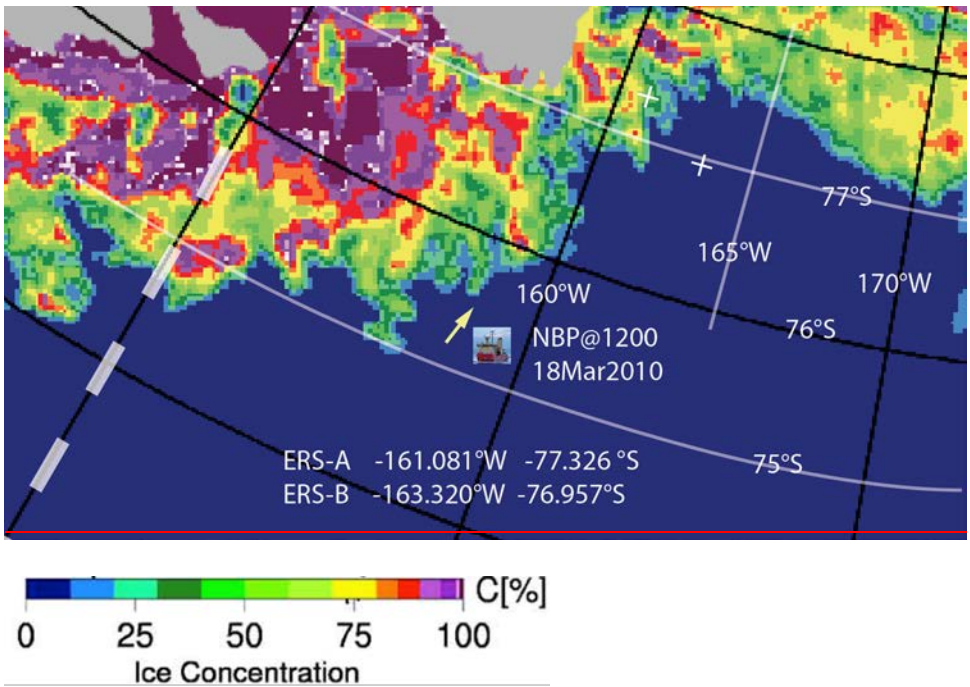

Fig. 25. Sea ice cover on March 18, 2011. The small white plus signs mark the locations of M1 (ERS-A) and M2 (ERS-B).

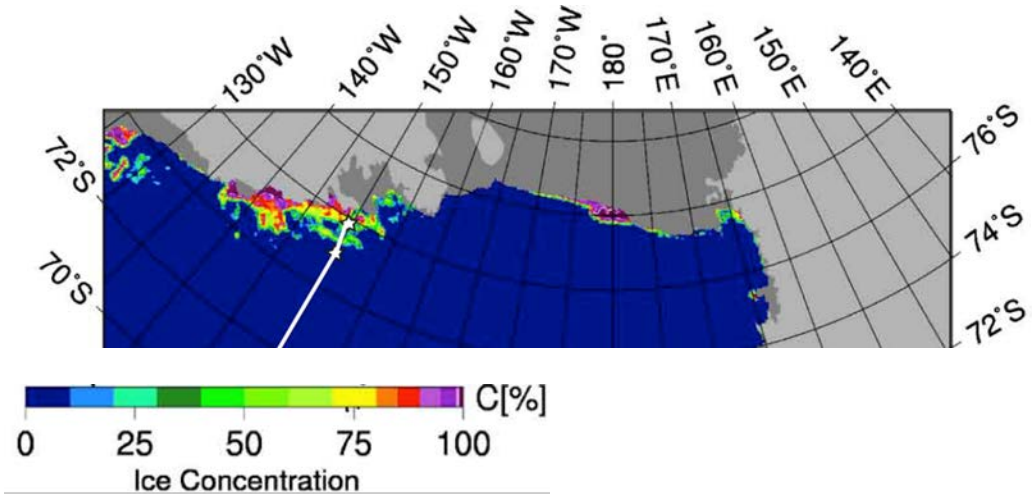

Fig. 26. Sea ice cover on February 21, 2011 in the summer season.

*Images are from the University of Bremem

Current velocity properties

The stick plots displaying the 40-hour low pass filtered current direction and speed record data can be found in Figure 27 for the current meters on M1 and M2. The yearlong current record displays a predominantly northward mean flow. The flow in M1 is more consistent than that observed for M2. Mooring 1 is mostly northward flowing, away from the ice shelf, and Mooring 2 is better distinguished by a predominant southward flow during the winter season. Figures 28 and 29 display the 30-day filtered rose plots summarizing the current records in degrees and magnitude.

The end of the melting season in the time series can be observed in the stick-plots for mooring 2 as a strong north and northeastward flow away from the shelf between February and April 2011. The current meters do not show much correlation between the instruments on both moorings. However, a curious feature of the record for both moorings is a relatively strong northward flow from February to March 2010 at the beginning of the time series. This period corresponds to the warming trend observed at both mooring sites. This contradicts what would be expected from at this time. During a warm, melting period, outflows from the ice shelf would be expected to reduce the temperature but instead an increase is observed. This may hint at some kind of warm current originating in the western Ross Sea that passes through this region occasionally or anomalously.

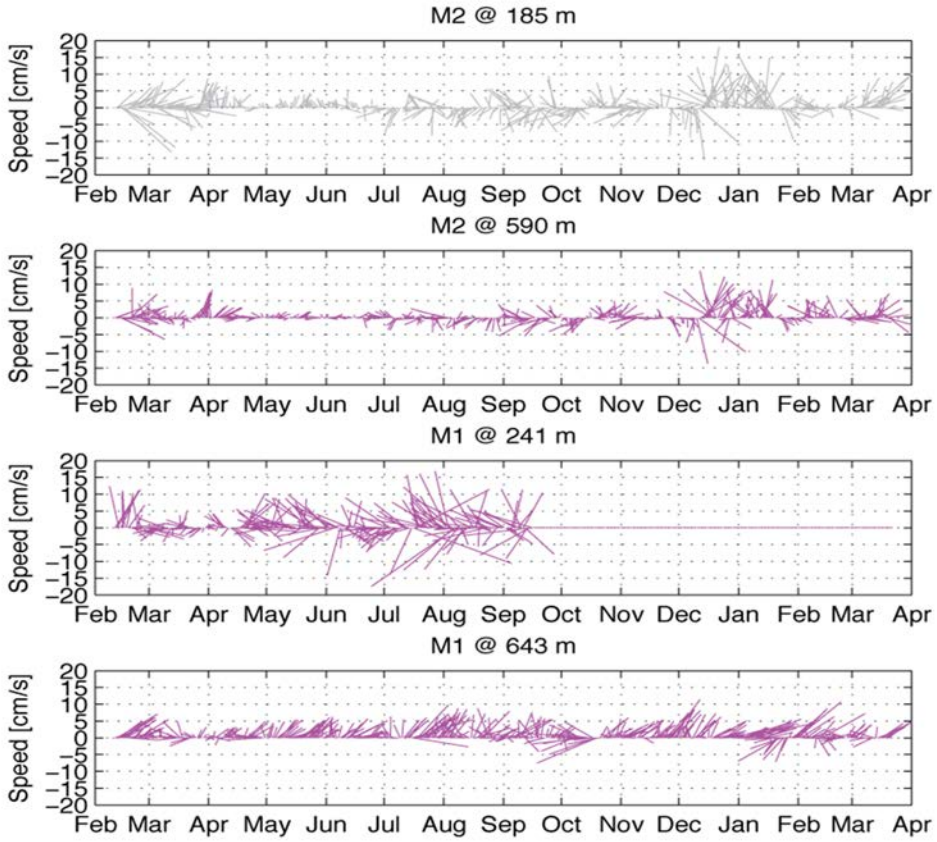

Fig. 27. These four panels show the 40-hour low pass filtered current meter record for the four current meters .

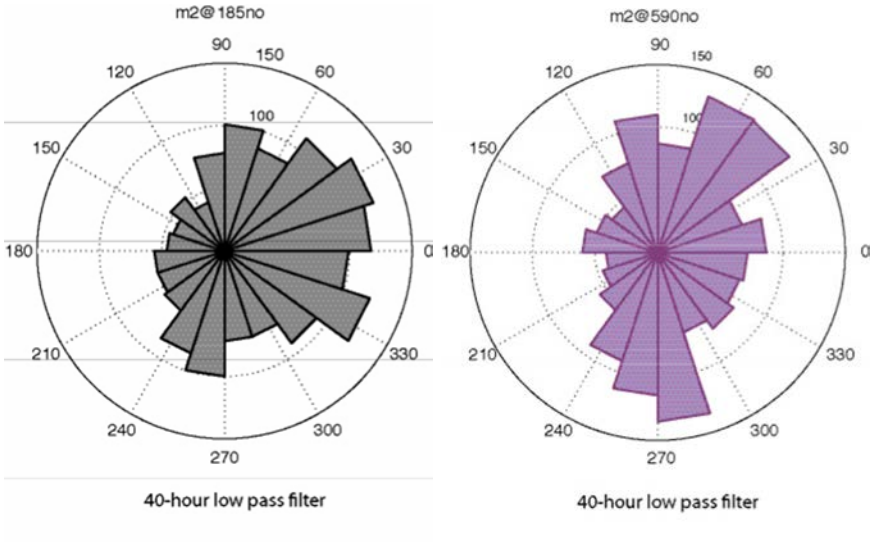

Fig. 28. The compass rose plots for the M2 current meters.

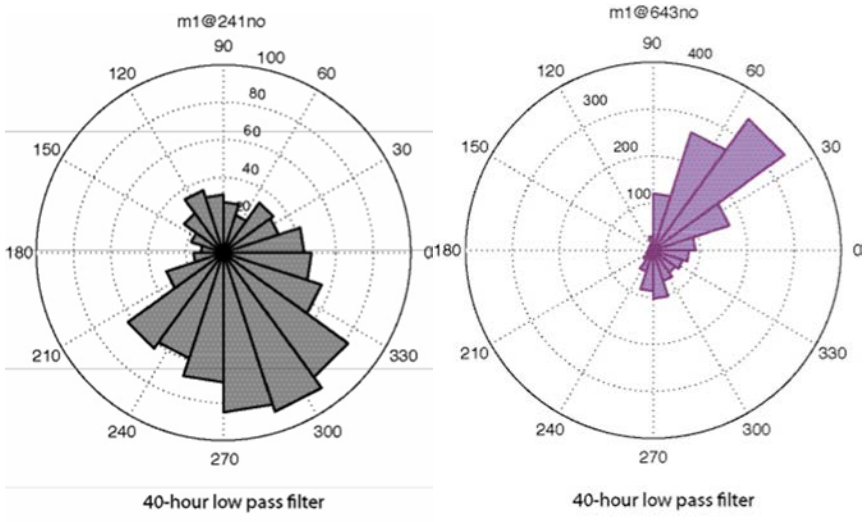

Fig. 29. The compass rose plots for the M1 current meters.

Conclusion

Antarctic Bottom Water has been observed forming in the Ross Sea during the past fifty years of hydrographic records and a remarkable concurrent long-term change in the salinity of most waters in the Ross Sea has been extensively reported during the same time period [*Jacobs and Giulivi*, 2010]. Determining the contributing influences to this dramatic ongoing freshening is of utmost relevance to the Meridional Overturning Circulation. Anomalies in salt content of upper waters imported from the Amundsen Sea are key to explaining the observed lightening of new AABW outflows further downstream in the central and western Ross Sea. Enhanced input of glacial meltwater with origins in the Amundsen Sea is expected along the Antarctic Slope and Coastal Currents. Measuring these changes facilitates the prediction of the extent and impact of global warming and other climate change phenomena, which are why studies such as these concerned with the acquisition and analysis of new data are imperative to Southern Ocean science.

REFERENCES

Assmann, K. M., Timmermann, R. *Variability of dense water formation in the Ross Sea*. *Ocean Dynamics* 55:2, 68-87, 2005.

Callahan, J. E. *The structure and circulation of deep water in the Antarctic. Deep-Sea Research*, 19, pp. 563-575, 1972.

Gille, S. T.. *Warming of the Southern ocean since 1950s*. *Science*, 295**,** 1275-1277, 2002.

Hellmer, H.H. & Jacobs, S.S. *Seasonal circulation under the eastern Ross Ice Shelf, Antarctica*. *Journal of Geophysical Research*,100, 10 873–10 885, 1995.

Jacobs, S. S., A. F. Amos, and P. M. Bruchhausen. *Ross sea oceanography and Antarctic bottom water formation*, *Deep-Sea Research*, Vol. 17 (6), 935-962, doi:10.1016/0011-7471(70)90046-X, 1970.

Jacobs, S. S. & Giulivi, C. F. *Large multi-decadal salinity trends near the Pacific-Antarctic continental margin*. *J. Clim.* doi:10.1175/2010JCLI3284, 2010.

Jacobs, S.S., R. G. Fairbanks, Y. Horibe. *Origin and evolution of water masses near the Antarctic continental margin: evidence from* $H_2{}^{18}O/H_2{}^{16}O$ *ratios in seawater Oceanology of the Antarctic Continental Shelf. Antarctic Research Series*, Vol. 43Am. Geophysical Union, Washington, DC (1985), pp. 59-85, 1985.

Kuhlbrodt, T., A. Griesel, M. Montoya, A. Levermann, M. Hofmann, and S. Rahmstorf , *On the driving processes of the Atlantic meridional overturning circulation*, *Rev. Geophys.*, 45, RG2001, doi:10.1029/2004RG000166, 2007.

Kwok, R. *Ross Sea ice motion, area flux, and deformation. Journal of Climate*, 18, pp.3759-3776, 2005.

Meredith, M. P. and A.M. Hogg. *Circimpolar response of Southern Ocean eddy activity to a change in the Southern Annular Model*. *Geophys. Res. Lett., 33,* **l**16608, doi:10.1029/2006GL026499, 2006.

Orsi, A. H. *Antarctic Crossroad of Slope Streams expedition aboard B. O. Puerto Deseado in the southwest Atlantic Ocean February – March 2009, Tech. Rep*. 09-01-T, Texas A&M University, College Station pp. 25, 2009.

Orsi, A. H., G. C. Johnson, and J. L. Bullister. *Circulation, mixing, and production of Antarctic Bottom Water*. *Progress in Oceanography*, *43*(1), 55- 109, doi:10.1016/S0079-6611(99)00004-X, 1999.

Rintoul, S., *On the origin and influence of Adélie Land Bottom Water, in Ocean, Ice and Atmosphere: Interactions at the Antarctic Continental Margin, Antarct. Res. Ser.*, vol. 75, edited by S. S. Jacobs and R. F. Weiss, pp. 151–172, AGU, Washington, D. C., 1998.

Talley, L. D., G. L. Pickard, W. J. Emery, and J. H. Swift. *Descriptive Physical Oceanography: An Introduction (6th edition).* Elsevier Science Inc., Boston., 2010.

Thompson, D. W.J. and S. Solomon. *Interpretation of recent southern hemisphere climate change*. *Science,* 296, 895-899, 2002.

Whitworth, T., A. Orsi, S-J Kim, W. Nowlin and R. Locarnini. *Water Masses and Mixing near the Antarctic Slope Front. Antarct. Res. Ser*. 75, 1-27, 1998.

CONTACT INFORMATION

Name:	Genevieve Victoria Genest
Professional Address:	c/o Dr. Alejandro H. Orsi Department of Oceanography O&M 616 MS 3146 Texas A&M University College Station, TX 77843
Email Address:	gene007@neo.tamu.edu
Education:	B.S., Environmental Geoscience, Texas A&M University, May 11, 2012 Undergraduate Research Scholar